Advanced Energy Conversion Materials
https://ojs.wiserpub.com/index.php/AECM/

UNIVERSAL WISER PUBLISHER

Research Article

Fabrication, Electrical Performance and Comparison of Ag/p-NiO/n-ITO/Ag, Ag/p-NiO/n-FTO/Ag, Ag/p-NiO/Glass/Ag Heterostructure Thin Films

Olcay Gençyilmaz[1*], İlker Kara[2], Ahmed Majeed Fadhil Alsamarai[3]

[1]Department of Material and Material Proceeding Technologies, Çankiri Karatekin University, Çankiri, Turkey
[2]Graduate School of Natural and Applied Sciences, Çankiri Karatekin University, Çankiri, Turkey
[3]Department of Physics, Institute of Science, Çankiri Karatekin University, Çankiri, Turkey
E-mail: ogencyilmaz@karatekin.edu.tr

Received: 10 February 2025; **Revised:** 26 March 2025; **Accepted:** 31 March 2025

Abstract: In this study, we fabricated and analysed heterostructure thin films based on nickel oxide (NiO) films using the low-cost successive ionic layer adsorption and reaction (SILAR) method. NiO films were deposited on three substrates: indium tin oxide (ITO), fluorine tin oxide (FTO) and glass. The structural, optical, electrical and surface properties of the NiO films were investigated, revealing that all films have a cubic crystal structure with grain sizes varying between 30-60 nm. The optical energy range of the films was determined to be between 3.56-4 eV by analysing their optical properties. Furthermore, it was observed that the use of ITO base in Ag/p-NiO/n-ITO/Ag heterostructure thin films significantly increased their transmittance values to approximately 40%. The *I-V* characteristics of Ag/p-NiO/n-ITO/Ag, Ag/p-NiO/n-FTO/Ag and Ag/p-NiO/Glass/Ag heterostructures were examined. The maximum barrier height (Φ_B) for the Ag/p-NiO/n-ITO/Ag heterostructure thin film was found to be 0.55 eV. In addition, the minimum ideality factor for this film was obtained to be 1.44 eV. The *I-V* analysis revealed that the Ag/p-NiO/n-ITO/Ag heterostructure is particularly suitable as a photoanode for solar cell applications.

***Keywords*:** NiO, indium tin oxide, fluorine tin oxide, Heterosturcture thin films, successive ionic layer adsorption and reaction method, electrical performance, photoanode

1. Introduction

Transparent conductive oxides (TCOs) are currently one of the most widely used materials in a variety of applications, including solar cells, touch screens, flat panel displays and light-emitting diodes (LEDs) [1]. The optical properties of TCOs can be tuned by controlling their composition, thickness and surface morphology, resulting in a wider range of applications than other materials [2]. Among TCOs, oxide semiconductors such as NiO, ZnO, TiO_2, SnO, MgO and CuO are among the most widely used materials in a variety of applications, including photodetectors, sensors, photodiodes and solar cells. In addition, these materials are also used in other areas such as sensing, catalysis and energy storage [3-6].

Nickel oxide (NiO) is a wide bandgap semiconductor with p-type conductivity (3.6 eV-4 eV) [7-9]. The wide bandgap of NiO makes it transparent in the visible region of the electromagnetic spectrum and opaque in the ultraviolet region. This property identifies it as a suitable candidate for applications in transparent conducting electrodes, solar cells

DOI: https://doi.org/10.37256/aecm.6120256539

and optoelectronic devices [10-12].

NiO films are produced by techniques such as magnetron sputtering, thermal evaporation, chemical bath deposition, pulsed laser deposition (PLD), spray pyrolysis, sol-gel and successive ionic layer adsorption and reaction [13-14]. Among these techniques, SILAR stands out due to its numerous advantages, including its practicality, cost-effectiveness and reproducibility. In particular, the substrate used in production significantly affects the physical properties of the films. In the literature, there are numerous studies on the use of substrates such as silicon, quartz; sapphire, glass, fluorine-doped tin oxide (FTO) and tin-doped indium oxide (ITO) in NiO production [15-18]. ITO is a highly degenerate n-type semiconductor and is used in the opto-electronics industry for a variety of applications including liquid crystal displays, light-emitting diodes, solar cells, gas sensors and touch screens [19-24]. FTO thin films represent a type of transparent conductive oxide film that has attracted great interest in recent years. FTO thin films consist of tin oxide crystal structures doped with fluorine atoms [25-27]. Their transparency and excellent electrical conductivity make them the most suitable material for use in optoelectronic devices such as solar cells and transparent electrodes in displays [28-35]. Despite the optical superiority of ITO substrates, FTO substrates have a higher thermal tolerance without a change in resistance value. This is useful for improving the efficiency of some devices that require higher annealing temperatures than ITO [36]. The absorbance of ITO substrates is different from that of FTO substrates and depends on the interaction of precipitates with these substrates. Also, the size of the particles formed causes increased scattering and reflection at some wavelengths and decreased absorption [37]. The transmittance of ITO substrates in the visible range is higher than FTO substrates due to the surface roughness of the FTO substrate [38]. FTO films have higher efficiency and are used as electrodes in some photovoltaic cells. They can also be used instead of high-cost ITO films [39]. Glass substrates are amorphous and enable epitaxial growth of NiO films, resulting in highly crystalline films. This can be advantageous for applications where high crystal quality is required, such as solar cells and gas sensors. ITO, FTO and glass bases are all widely used in different production techniques. ITO in particular has advantages over other bases with its features such as low resistance, high current carrying capacity and high transmittance. The selection of these bases depends on cost, conductivity, permeability, chemical and thermal properties. Determining the appropriate base before production is extremely important depending on the desired properties.

The effect of the substrates used in the production of NiO films by SILAR on the properties of the films has not been fully explained in the literature. The contribution of our study to the literature is to elucidate the effects of the base used on the structural, optical, surface and electrical properties of NiO films to be produced in order to determine their potential for use as photoanodes. For this aim, NiO heterostructured thin films were deposited on three different susbtrates (ITO, FTO and glass) using the SILAR method. Structural, surface, optical and electrical properties of p-n heterostructured thin films obtained by using different substrates were investigated and the effects of the base used on the properties of NiO films were determined. The NiO-ITO films exhibited significant properties as the most suitable substrate for the SILAR technique with a low ideality factor and high crystallisation level.

2. Material and method

2.1 *Substrate preparation*

ITO, FTO and glass materials were used as the substrate for the growth of the films. The glass substrates were cut to 8 mm wide and 25 mm long. After the cutting process, the glass substrates, FTO, ITO, and glass were washed thoroughly with soapy water to get rid of dirt. After washing, the substrates were ultrasonically cleaned in acetone for 10 minutes. The clean FTO, ITO, and glass substrates were then dried in nitrogen gas. All processes were performed at room temperature.

2.2 *Solutions preparation*

Solutions were prepared to obtain nickel oxide layers by dissolving nickel (II) nitrate and aqueous ammonia in distilled water in a flask (one hundred milliliters) to obtain a ketone precursor and form compound ions ($[Ni(NH_3)_4]^{+2}$) with (pH ≈ 10), where the reagents are used analytically for $Ni(NO_3)_2$ and concentrated ammonia (NH_3) (28%). The specific concentration values for a nickel (Ni) solution were 0.1 M and the molar ratio of Ni : NH_3 was 1 : 10 obtained

as a result of several experiments. The SILAR growth cycle consists of four successive steps:

(i) Dipping the substrate into the ($[Ni(NH_3)_4]^{+2}$) complex solution for 30 seconds to create a thin liquid film containing ($[Ni(NH_3)_4]^{+2}$) on the substrate; (ii) immediately dipping of the extruded substrates into hot water (90 °C) for 7 seconds to form a NiO layer; (iii) dry the substrates in the air for 60 sec and (iv) then keep them in distilled water at room temperature for 30 minutes. Thus, the SILAR cycle is completed. The diagram showing the precipitation steps with the SILAR method to obtain nickel oxide films is shown in Figure 1. The process was repeated 40 times for all samples under the same conditions and annealing temperature for 15 minutes in an annealing furnace. The thickness of the produced films was determined by the weight method and calculated as approximately 200 nm for NiO-Glass, NiO-FTO and NiO-ITO films.

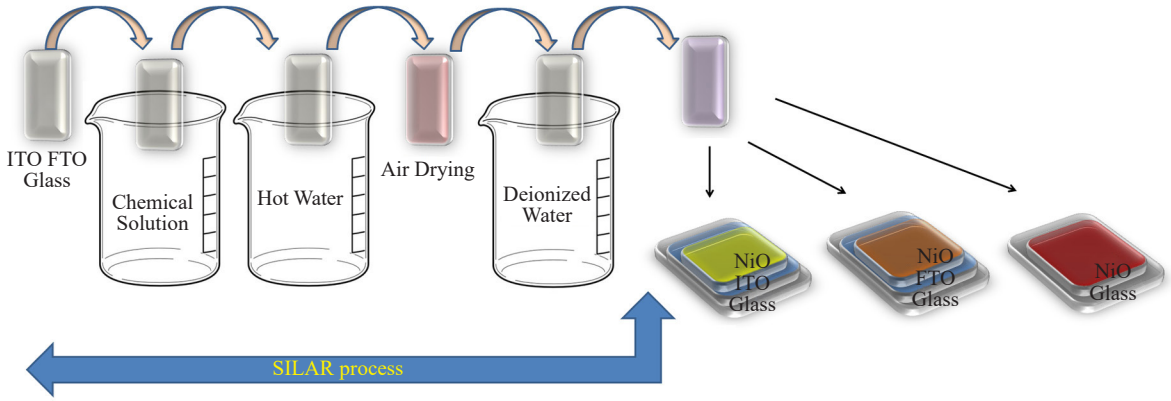

Figure 1. Diagram representing the steps of sedimentation by the SILAR method

2.3 *Characterization techniques*

The structural, optical, electrical and surface properties of NiO-ITO, NiO-FTO and NiO-Glass films deposited on different substrates were investigated. The characterisation of these properties was conducted using a range of analytical techniques, including X-ray diffraction (XRD), ultraviolet-visible (UV-VIS) spectrophotometry, current-voltage measurement (*I-V*) and field emission scanning electron microscopy (FESEM). The UV-VIS spectrometer was employed for optical analysis. Absorbance and transmittance spectra were obtained from UV-vis spectrometer analyses. These spectra were used to determine the band gap, band structure, Urbach energies, refractive indices, and transmittance of NiO films. An APD 2000 PRO XRD device was used to analyse the X-ray results. X-ray diffraction patterns of NiO films were obtained from XRD analysis. The crystallisation levels, grain sizes, lattice constants, half-peak widths and dislocation densities of the NiO films were calculated using the obtained X-ray diffraction patterns. The electrical properties of the films were determined by the two-end method. This involved making an Ag contact at two different points on the films, applying voltages in the range of -3 and +3 volts, and determining the current values against these voltages. A schematic representation of the contacts for *I-V* measurements is provided in Figure 2. *I-V* graphs were constructed from the obtained current (*I*)-voltage (*V*) values, and the transmission mechanisms were determined. In addition, electrical parameters such as barrier height and ideality factor of NiO films were also calculated. The field emission scanning electron microscopy (FESEM) characterisation technique was employed to investigate the morphological properties and the effect of the base used on the surface properties of the films. The surface images of the films were obtained in general, and the effect of the substrate used on the surface properties was examined.

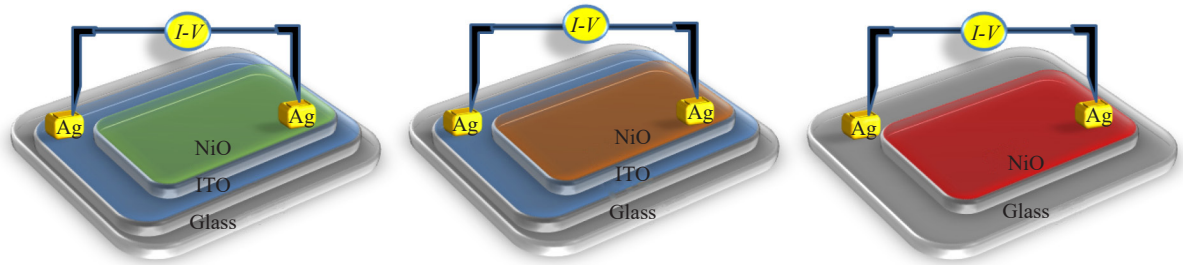

Figure 2. Illustration of Ag/p-NiO/n-ITO/Ag, Ag/p-NiO/n-FTO/Ag, Ag/p-NiO/Glass/Ag heterostructure thin films

3. Results and discussion

3.1 *Structural properties*

Structural analysis of the NiO films was conducted using a CuK_{α} radiation source with a wavelength of $\lambda = 1.54056$ Å. The diffraction patterns were recorded by varying the diffraction angle (2θ). From the XRD data, the structural parameters such as crystalline level, dominant orientations, lattice constants (a, b, and c), grain size (D), dislocation density (d), FWHM, and micro stress (ε) were calculated for all films using the following equations. Figure 3 displays the XRD patterns for NiO-ITO, NiO-FTO, and NiO-Glass films. Analysis revealed that NiO-ITO exhibits the highest level of crystallization among all NiO films. NiO-Glass films exhibit the lowest crystallization level compared to the other films. While the crystallization level of NiO-FTO films is lower than that of NiO-ITO films, it is better than that of NiO-Glass films. The distances between the crystalline plane (d) values detected through XRD results of the NiO films show good conformity with the standard (d_0) values. The films were recognized to be produced in NiO's cubic phase according to the Joint Committee on Powder Diffraction Standards card (JCPDS: 01-073-1519), and the diffraction peaks were distinguished. In addition, the primary growth orientation in all films was in the (111), (200) and (220) directions and averaged over these three peaks, the lattice constants of NiO-Glass, NiO-ITO and NiO-FTO films were determined as $a = b = c = 4.165°$, $a = b = c = 4.157°$ and $a = b = c = 4.154°$, respectively (Table 1).

Table 1. Some structural parameters of NiO-ITO, NiO-FTO, NiO-Glass heterostructure thin films

Material	2θ (°)	FWHM (~)	d (Å)	Grain size (nm)	ε (Lines^{-2}nm^{-4})	δ (Lines/nm^2)	Lattice parameter (Å) $a = b = c$
NiO-Glass	37.35	0.1629	0.240	51.4	6.70×10^{-5}	3.77×10^{-4}	4.165
	43.39	0.290	0.208	29.4	1.17×10^{-4}	1.15×10^{-3}	
	62.59	0.1555	0.148	59.7	5.70×10^{-4}	2.80×10^{-4}	
NiO-FTO	37.45	0.174	0.239	48.1	7.10×10^{-4}	4.31×10^{-4}	4.154
	43.66	0.260	0.207	32.8	1.05×10^{-3}	9.26×10^{-4}	
	63.06	0.161	0.147	57.6	5.90×10^{-4}	3.01×10^{-4}	
NiO-ITO	37.45	0.250	0.239	33.4	1.03×10^{-3}	8.94×10^{-4}	4.157
	43.48	0.290	0.207	29.4	1.17×10^{-3}	1.15×10^{-4}	
	62.71	0.254	0.147	36.5	9.40×10^{-3}	1.00×10^{-4}	

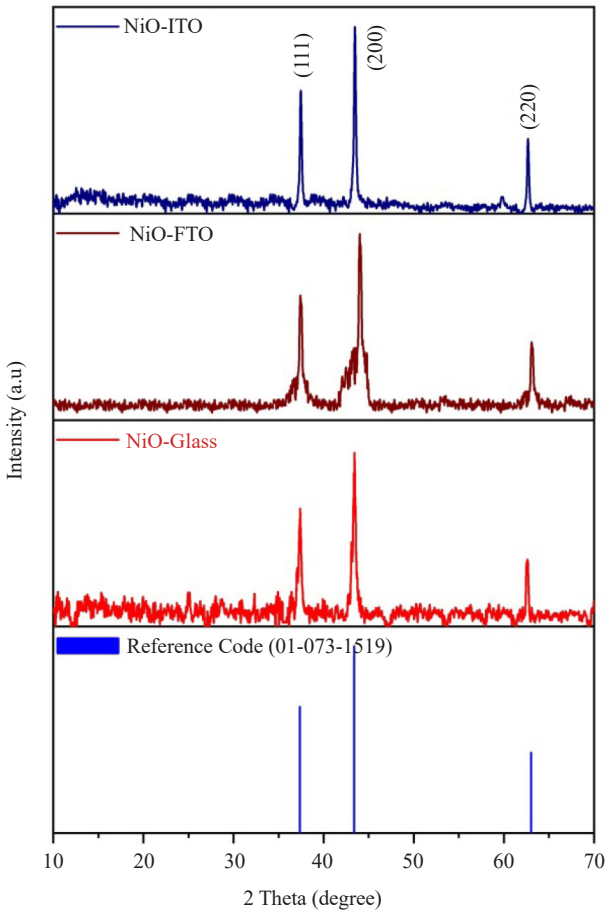

Figure 3. XRD spectra of NiO-ITO, NiO-FTO and NiO-Glass heterostructure thin films

Some structural parameters of NiO films, including diffraction angle (2θ), interplanar distance (d), full width at half maximum (FWHM), grain size (G), micro strain (ε) and dislocation density (δ) were determined. The grain size, dislocation density and micro strain (ε) of the NiO films were calculated using the following formulas, respectively [40-42].

$$D = \frac{0.9\lambda}{\beta \cos\theta} \tag{1}$$

$$\delta = \frac{1}{D^2} \tag{2}$$

$$\varepsilon = \frac{\beta \cos\theta}{4} \tag{3}$$

where λ is wavelength, β is full width at half maximum, θ is Bragg angle and D is grain size. These findings are presented in Table 1 for the NiO-Glass, NiO-FTO, and NiO-ITO heterostructure thin films.

3.2 *Optical properties*

The response of NiO films to visible light was established through the utilisation of UV-Vis spectroscopy, in conjunction with various optical parameters, including band gap, Urbach energy and refractive index. Absorbance and transmittance spectra were recorded for all materials in the range of 200-1,100 nm. The transmittance and absorbance spectra for NiO films are exhibited in Figure 4a and b, respectively. The material with the highest average transmittance value in the visible region was NiO-ITO, while the lowest material was NiO-Glass. It has been demonstrated that ITO bases are more suitable than others to obtain high transmittance values in NiO films. When the absorption spectra are examined, it is evident that the band edge of the NiO-glass films has a more flat and distorted structure. This situation is slightly improved for NiO-FTO, with the films exhibiting smoother band edges than NiO-glass. Conversely, it was determined that the band edge of NiO-ITO films became sharper, with the band structure improving. Additionally, a graph illustrating the change in refractive index values of NiO films according to wavelength is presented in Figure 4c. It was determined that the average refractive index values of the films in the visible region ranged between 1.5 and 2.

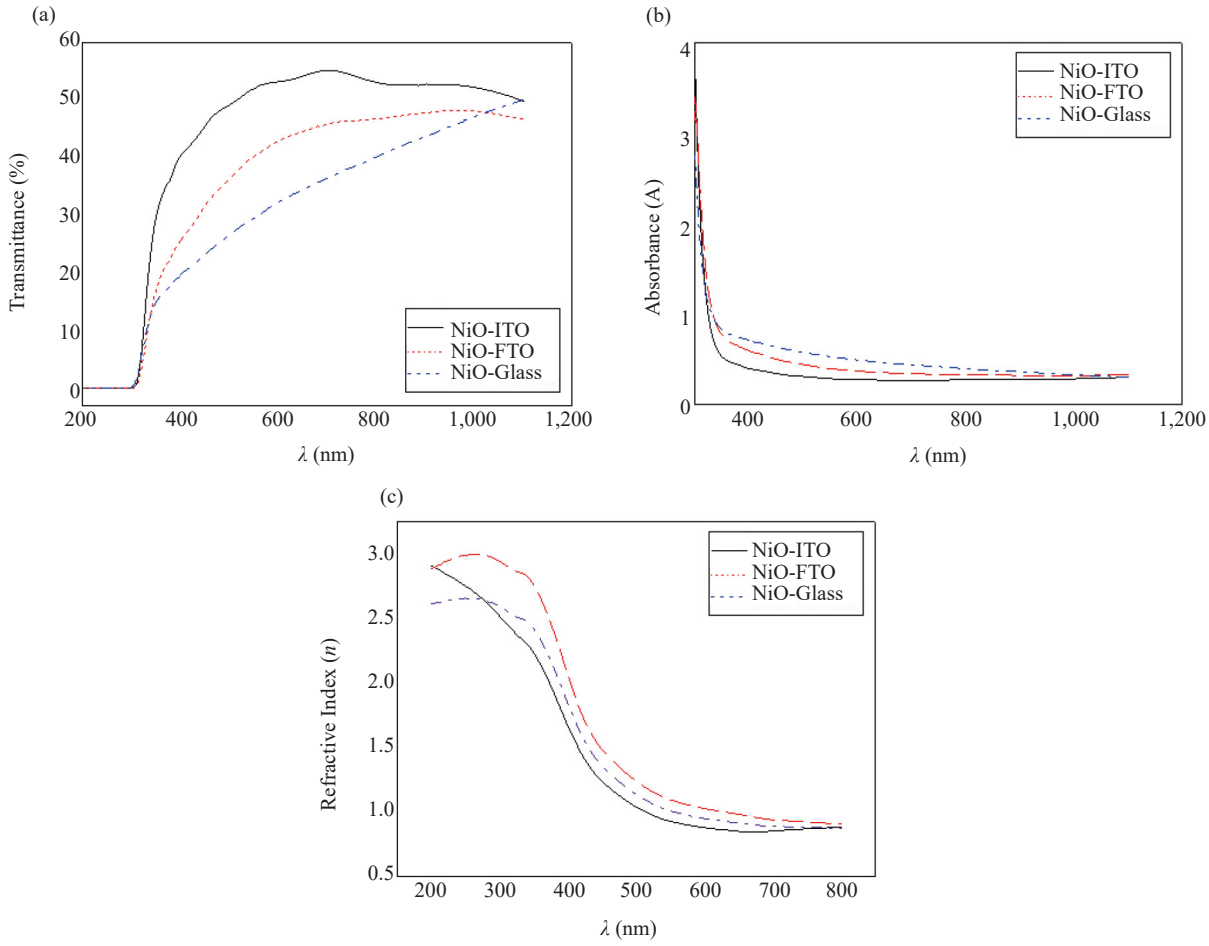

Figure 4. (a) Transmittance, (b) Absorbance and (c) Refractive index spectra of NiO-ITO, NiO-FTO, and NiO-glass heterostructure thin films

For the optical band gap values calculation of NiO films was used to the following Tauc equation [43]:

$$(\alpha hv) = A(hv - E_g)^n \quad (4)$$

where A is a constant determined by the refractive index of the material, E_g represents the optical band gap, and hv is

the photon energy. Figure 5 shows the optical energy gap of NiO films for direct and indirect electron transitions. While the calculated indirect optical energy gap value was in the range of 3.56-3.68 eV, the direct optical energy gap values were determined to be in the range of 3.92-3.97 eV. The calculated band gap energy values of NiO films produced on ITO, FTO and glass are 3.91, 3.93 and 3.97 eV, respectively. Band gap values of NiO films produced on ITO and FTO substrates are almost the same. However, band gap values of NiO films produced on glass are higher than films produced on other substrates. NiO films produced on glass substrates have the widest band gap 3.97 eV for direct band transition.

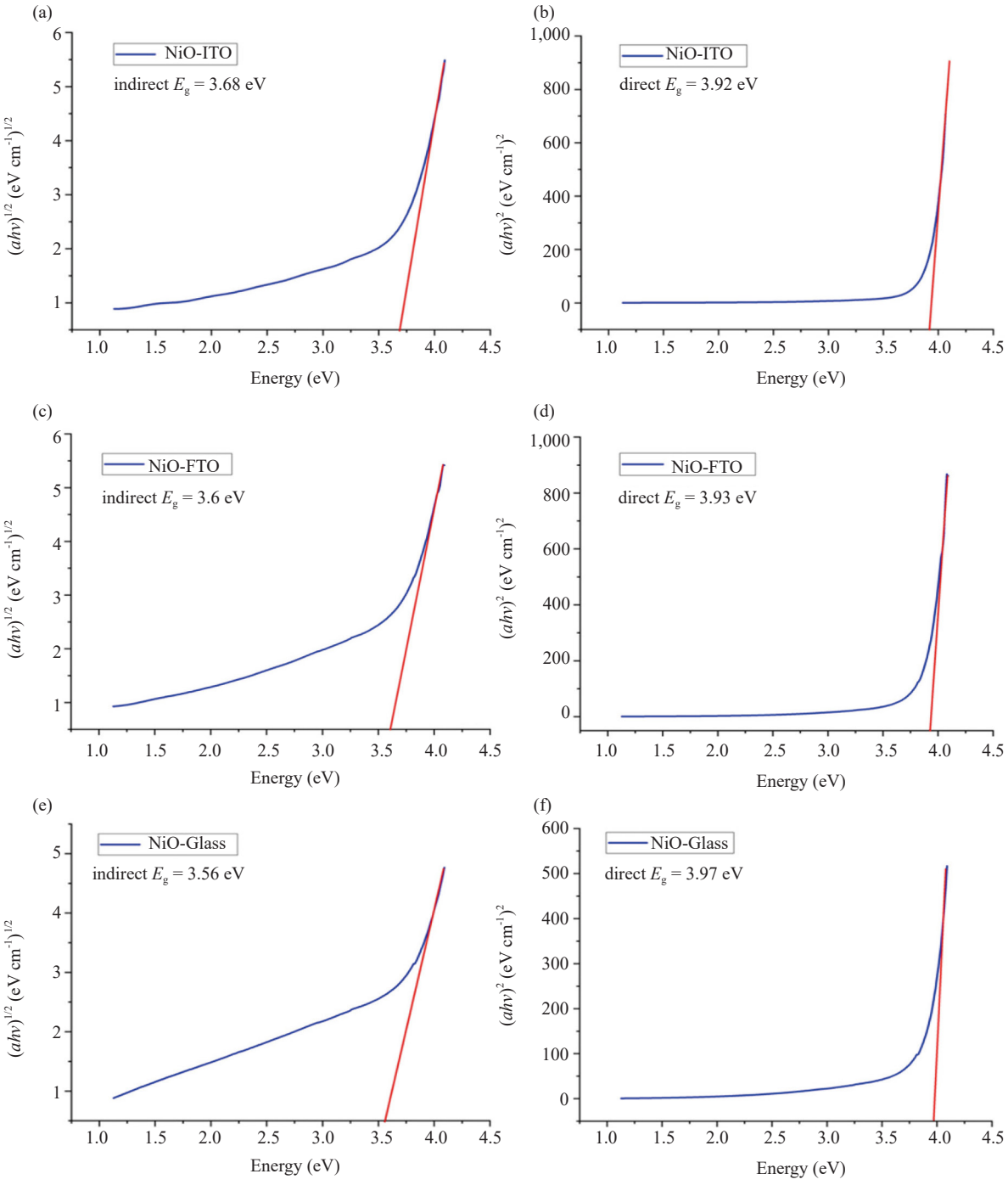

Figure 5. The *ahv-hv* graphics of NiO films

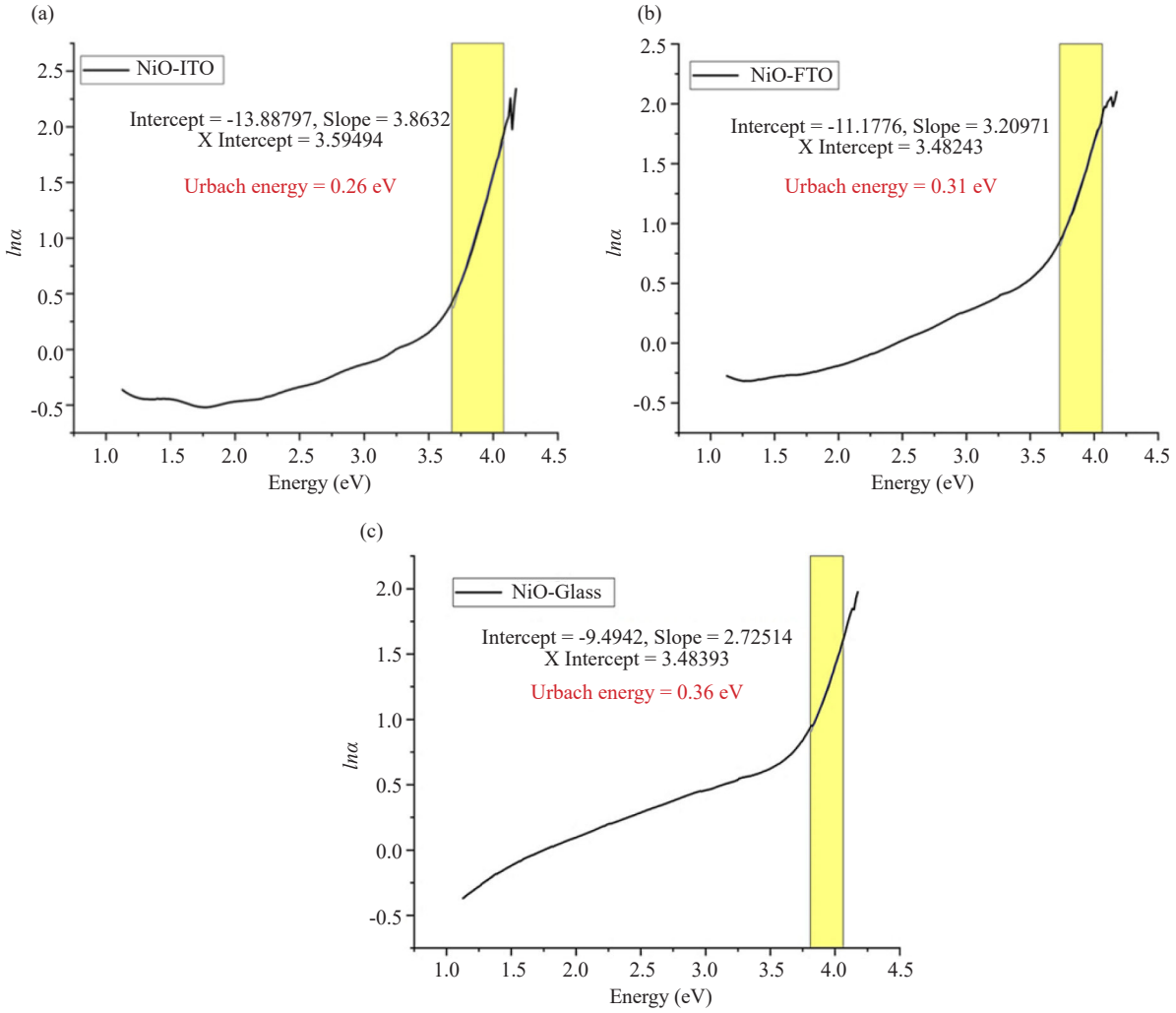

Figure 6. Urbach energy (a) NiO-ITO, (b) NiO-FTO and (c) NiO-Glass films

Optical transitions between a material's valence and conduction bands, defect states, conduction mechanisms, and disproportionate charge-induced defects depend on the material's bandgap. The identification of these changes and defects in the structure is achieved by detecting the Urbach tails that are formed in the band structure. The energy associated with these Imperfect Urbach tails in the band structure is referred to as the Urbach Energy (E_u). Therefore, it is a significant parameter in identifying alterations in the band structure of materials. The Urbach energy was determined by computing the inverse of the gradient of *lnα-hv* plots, using the following equation [44]:

$$\alpha = \alpha_0 \exp^{hv - E/E_u} \tag{5}$$

where α_0 is a constant and E_u represents the Urbach energy, which is the width of the tails of localized states in the material's band gap. *lnα-hv* graphs are presented in Figure 6. The Urbach energy of NiO-ITO films is higher than that of NiO-Glass films. This change indicates improved crystallisation of NiO-ITO films and fewer defects in these films. XRD results support this situation (Figure 3). The base on which NiO films are grown significantly affects the structural and surface properties of the films. Therefore, better crystallisation and more homogeneous surface distribution on ITO substrates, which are more regular than glass substrates, cause better optical parameters of NiO-ITO films. Also, surface defects in semiconductor films can significantly affect electronic band structures, leading to changes in optical, electrical and transport properties. These defects introduce localised states in the bandgap, alter carrier dynamics and can even

change the effective bandgap. Surface irregularities and imperfections effectively widen the band edges, creating Urbach sagging. This can lead to valance band gap absorption. However, imperfections can also lead to surface reorganisation by causing structural changes that alter the surface band distribution. The higher Urbah energy of NiO-Glass films may be due to the surface properties mentioned in these reasons. FESEM images (Figure 7) support this situation. Cracks, surface irregularities and defects on the surface of NiO-Glass films effectively widened the band edges and caused Urbach tailing.

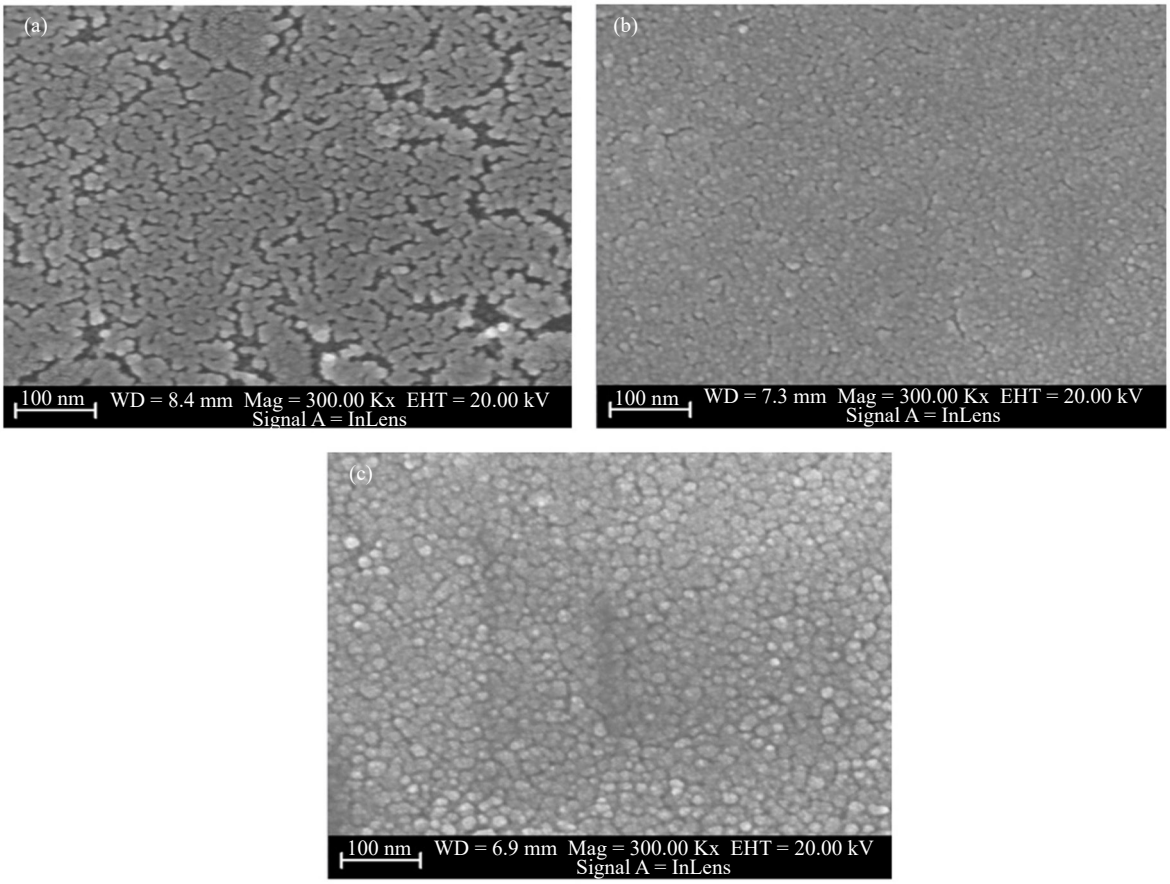

Figure 7. FESEM images of (a) NiO-Glass, (b) NiO-FTO and (c) NiO-ITO heterostructure thin films

Another important parameter showing the change in the band structure is the steepness (σ) parameter. This parameter is the perpendicularity parameter that shows the band broadening in the material. Also, the step parameter determines the electron-phonon ($E_{e\text{-}p}$) interaction. These two important parameters can be calculated with the following equations [45, 46]:

$$\sigma = \frac{k_B T}{E_u} \tag{6}$$

where σ is the steepness parameter, k_B is the Boltzmann constant, and T is the absolute temperature. These calculated values and changing are given in Table 2 and Figure 8.

Table 2. Some optical parameters of NiO-ITO, NiO-FTO and NiO-Glass films

Films	Direct E_g (eV)	Indirect E_g (eV)	E_u (meV)	$\sigma \times 10^{20}$	$E_{e\text{-}p} \times 10^{19}$
NiO-ITO	3.92	3.68	260	1.44	4.59
NiO-FTO	3.93	3.60	310	1.21	5.48
NiO-Glass	3.97	3.56	360	1.04	6.36

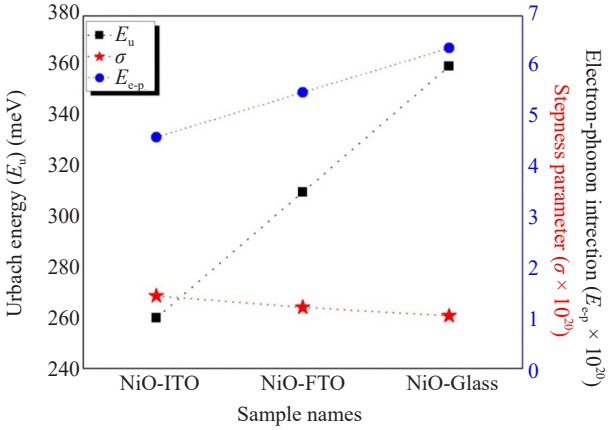

Figure 8. Change of Urbach energy (E_u), steepness parameter (σ) and electron-photon interaction ($E_{e\text{-}p}$) values

3.3 *Electrical properties*

The two-point method was utilised in order to examine the sheet resistance (R_s). A variation in the voltage (V) was applied between the outer two leads and the current (I) was measured under dark conditions. The reverse to forward bias current measurement was taken for the applied potential of -3 V to +3 V. This method was applied linearly, and the layer resistance was calculated. Figure 9 shows the I-V characteristics of nio heterostructure thin films under dark conditions. The graph and the values of the surface resistance demonstrated that NiO-glass films deposited on glass substrates exhibited linear ohmic behaviour in both cases of forward and reverse bias, as illustrated in Figure 9a. In contrast, the NiO-FTO films exhibited nonlinear behaviour closer to exponential than ohmic behaviour in both forward and reverse bias cases. The films of NiO-ITO and NiO-FTO exhibited diode properties, as shown in Figure 9b-c.

We had defined R_s is the surface resistance when d thickness of the film it is the ratio between the electrical resistance ρ. Resistance is symbolized by the symbol R_s and its unit (Ω) and it is expressed by the following equations [47]:

$$R_S = \rho / d \tag{7}$$

$$R_S = \frac{\pi V}{\ln 2 I} \tag{8}$$

where is I is electric current (A), V is fitted voltages and π/ln2 is the correction factor is equal to 4.532. Also, the electrical conductivity σ values calculate using by the following equations:

$$\sigma = \frac{1}{\rho} \tag{9}$$

$$\rho = \frac{\pi}{\ln 2} d \frac{\mathrm{V}}{\mathrm{I}} \tag{10}$$

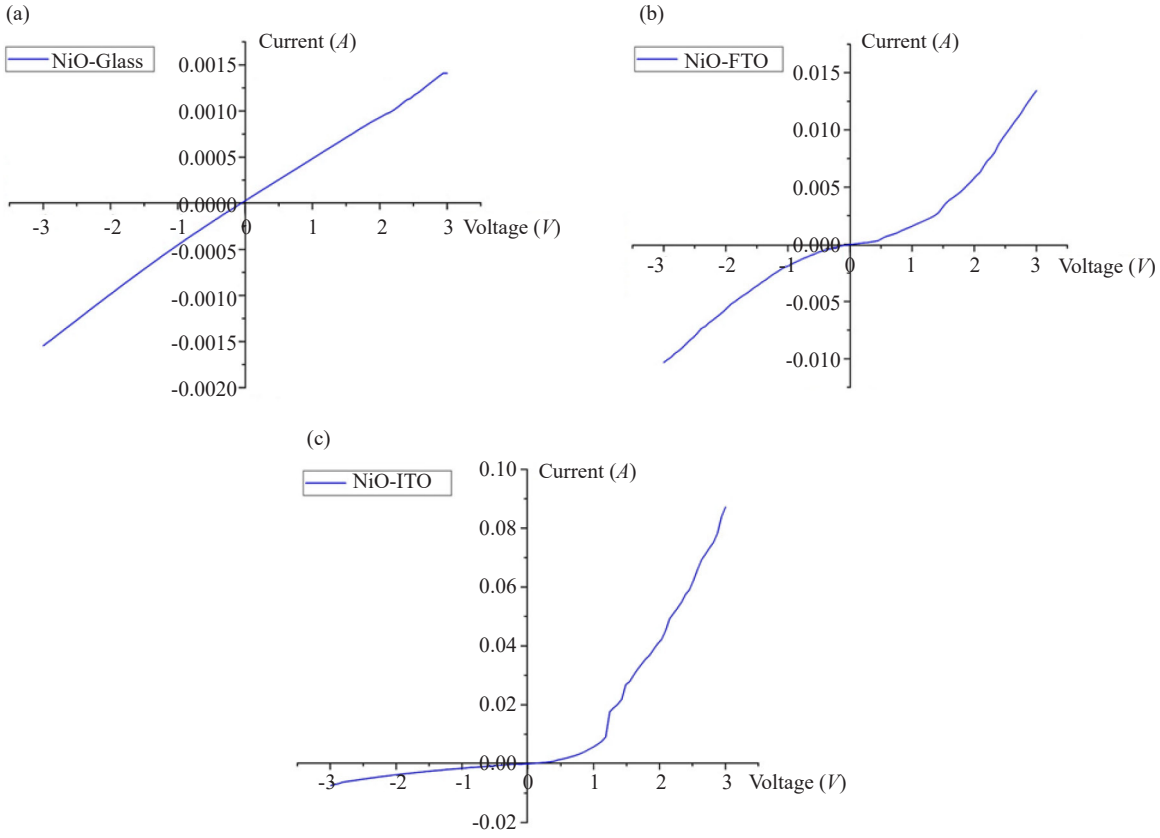

Figure 9. Voltage and current curve of (a) NiO-Glass, (b) NiO-FTO and (c) NiO-ITO heterostructure thin films

The *I-V* results indicate that the surface resistance and electrical conductivity values of the films are presented in Table 3. It can be observed that the conductivity of the NiO-ITO and NiO-FTO films is higher than that of the NiO-Glass film in both the forward and reverse bias of conductivity. This increase in conductivity can be attributed to the tail width of localized states within the optical bandgap (Urbach energy), which is dependent on the nature of the substrate used. Furthermore, alterations to the crystal structure of the films may result in enhanced electrical conductivity.

Table 3. The surface resistance values in the forward and reverse bias

Material	Forward bias			Reverse bias		
	V (Volt)	(Ω)	*σ* (Ω·cm)	*V* (Volt)	(Ω)	*σ* (Ω·cm)
NiO-ITO	3-0.05	7.32×10^{2}	6.83×10^{1}	(-3)-(-0.05)	2.68×10^{3}	1.87×10^{1}
NiO-FTO	3-0.05	2.88×10^{3}	1.73×10^{1}	(-3)-(-0.05)	6.17×10^{3}	8.10
NiO-Glass	3-0.05	9.26×10^{3}	5.40	(-3)-(-0.05)	9.77×10^{3}	5.12

To determine the charge transport mechanism of the NiO films, a conventional current Eq. (11) is used as;

$$I = I_0\left[\exp\frac{qV}{nkT}\right] \tag{11}$$

where V is the applied voltage, n is the ideality factor, k is the Boltzmann constant, T is the absolute temperature and q is the electronic charge, I_0 is the saturation current. I_0 is the saturation current given by Eq. (12);

$$I_0 = AA^*T^2\exp\left(-\frac{q\phi_B}{kT}\right) \tag{12}$$

where A, A*, are the zero-bias barrier height, effective contact area and effective Richardson's constant respectively. The theoretical value of Richardson's constant is expressed as in Eq. (13).

$$A^* = \frac{4\pi m^* K^2 q}{h^3} \tag{13}$$

where h is the Planck's constant and m* is the effective mass of electron. Here we put $m^* = 0.8\ m_0$ for NiO to get the value of effective Richardson's constant, and the calculated value was found to be $A^* \sim 96$ A-cm^{-2}-K^{-2} [48].

The NiO film parameters barrier height φ_B and ideality factor η were measured under dark conditions. The reverse to forward bias current measurement was taken for the applied potential of -3 V to +3 V. By using the theory of thermoionic emission and using I-V results of the deposited films, the parameters barrier height φ_B, ideality factorwere measured by the following Eq. (13) and (14):

$$\varphi_B = \frac{K_b T}{q}\ln\left(\frac{AA^*T^2}{I_0}\right) \tag{14}$$

where φ_B is barrier height at zero bias. The ideality factor (η) which is another important electrical parameter were calculated by the following;

$$\eta = \frac{q}{K_b T}\left(\frac{dV}{d(\ln I)}\right) \tag{15}$$

The log I-V plots of NiO films is given in Figure 10 and Could $\left(\frac{dV}{d(\ln I)}\right)$ obtained from the I-V graph in these graphs. And we got the η valuses [49]. Table 4 shows some electrical parameters calculated. These results are roughly consistent with previous studies [50-52]. The films (NiO-ITO) and (NiO-FTO) showed slightly different electrical behvior than the other samples, as this sample has characteristics close to a diode and a small saturation current compared to the other samples as shown in the Figure 10. The lowest ideality factor was observed in the NiO-ITO thin film, while the highest ideality factor was observed in the pure NiO-Glass thin film. This can be attributed to the improvement of the surface morphology of the NiO-ITO thin film. It has been shown that NiO-ITO films exhibit superior electrical properties compared to other films and similar studies are found in the literature [53-55].

Table 4. The calculated barrier height φ_B, ideality factor η parameters

Films	η	φ_B (eV)
NiO-ITO	1.4420	0.554
NiO-FTO	1.9756	0.494
NiO-Glass	3.4480	0.589

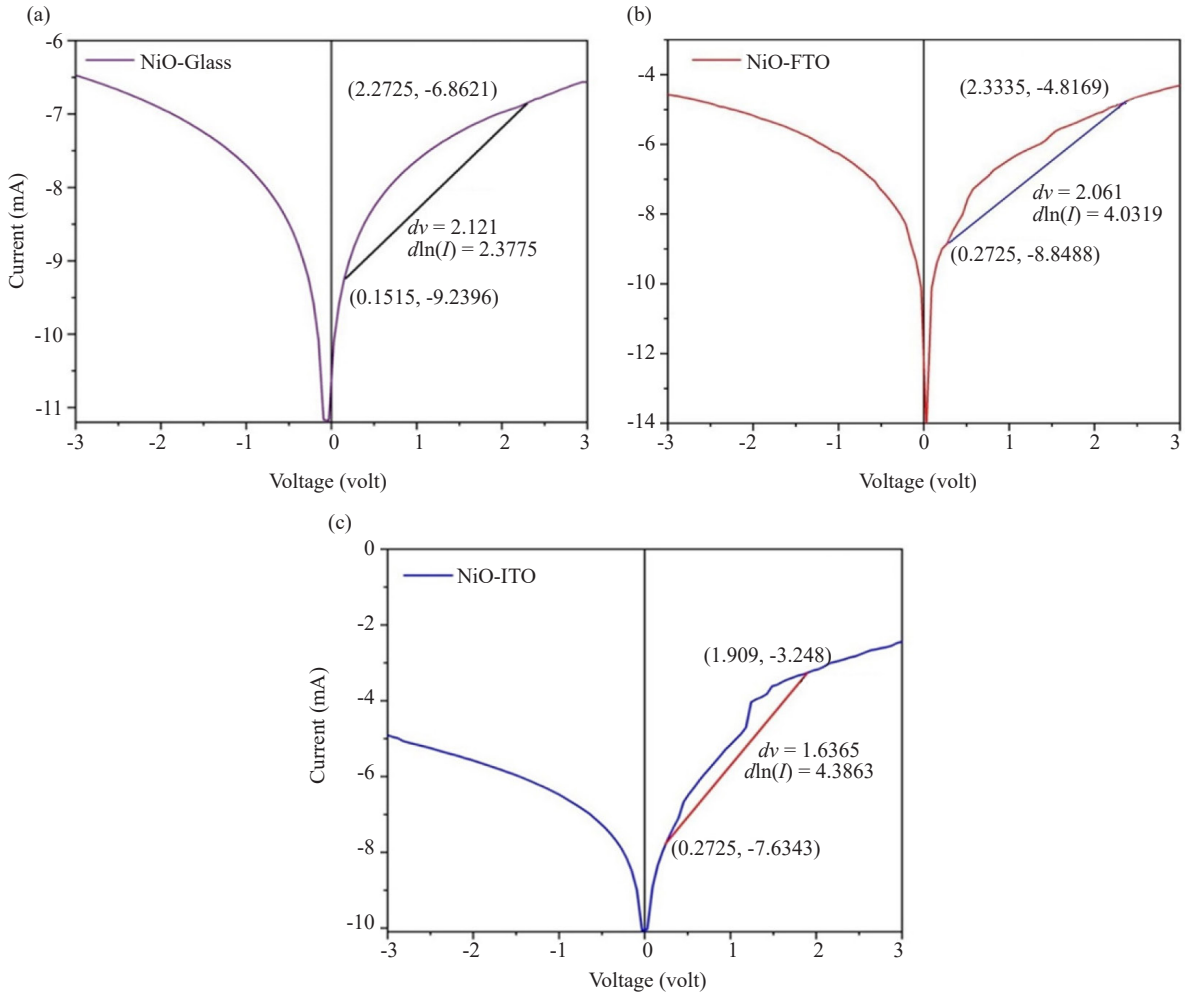

Figure 10. The log *I-V* plots of (a) NiO-Glass, (b) NiO-FTO and (c) NiO-ITO heterostructure thin films

3.4 *Surface properties*

A field emission scanning electron microscope (FESEM) was employed to examine the surface morphology of the films NiO-Glass, NiO-FTO, NiO-ITO deposited on substrates. Figure 7 shows FESEM images of the deposited films. It is evident that the surfaces of the prepared films exhibit round particles, with a homogeneous distribution on the substrate, and that there are no cracks on the surface of the film or large molecular agglomerations. The formation of the film surface is contingent upon the method of preparation and deposition parameters of the SILAR method. The surface homogeneity of the films deposited on the FTO and ITO substrates was determined to be superior to that of the NiO films deposited on the glass substrate. While cracks were observed in some areas of the surfaces of the films deposited

on the glass, other films exhibited complete homogeneity. The most homogeneous NiO films were those deposited on ITO. In all films, Ni and O atoms combine to form a round structure. In NiO films produced on ITO base, these round formations are more prominent and larger than in other films.

4. Conclusions

NiO-ITO films have high crystallinity levels, low grain size, more stable and homogeneous surface morphology. They have higher optical transmittance (60%) and a more suitable band structure compared to other films. NiO-ITO films showed high electrical conductivity (6.83×10^{1}-1.87×10^{1} Ω·cm), lowest saturation current and diode behavior. Also, these films have the lowest ideality factor (1.44). These results show that the ITO base material used in the production of NiO films produced by the SILAR method will significantly increase the quality of the films compared to FTO and glass bases and expand their potential applications. Especially, NiO-ITO heterostructured films have the potential to be used as photoanodes in solar cells and photodetectors.

Acknowledge

This study is produced from the Master thesis "Production and Characterization of Heterostructured NiO/FTO-NiO/ITO-NiO/Glass Films" prepared by Ahmed Majeed Fadhil Alsamarai in 2023 under the supervision of Assoc. Prof. Dr. Olcay GENÇYILMAZ.

Authors contribution

Olcay Gençyilmaz: Conceptualization, Methodology, Validation, Data curation, Writing-review & editing, Writing-original draft, Supervision.

İlker Kara: Methodology and Writing-original draft.

Ahmed Majeed Fadhil Alsamarai: Methodology and Writing-original draft.

Data availability

Data will be made available on request.

Conflict of interest

The authors declare that they have no known competing financial interests or personal relationships that could have appeared to influence the work reported in this paper.

References

[1] Exarhos GJ, Zhou XD. Discovery-based design of transparent conducting oxide films. *Thin Solid Films*. 2007; 515(18): 7025-7052.

[2] Søndergaard RR, Hösel M, Krebs FC. Roll-to-Roll fabrication of large area functional organic materials. *Journal of Polymer Science Part B: Polymer Physics*. 2013; 51(1): 16-34.

[3] Caporaletti O. Electrical and optical properties of bias sputtered ZnO thin films. *Solar Energy Materials*. 1982; 7(1): 65-73.

[4] Napari M, Huq TN, Hoye RLZ, MacManus Driscoll JL. Nickel oxide thin films grown by chemical deposition

techniques: Potential and challenges in next generation rigid and flexible device applications. *InfoMaterial and Technology Science*. 2021; 3(5): 536-576.
[5] Chavillon B. *Synthèse et caractérisation d'oxydes transparents conducteurs de type p pour application en cellules solaires à colorant [Synthesis and Characterization of p-Type Transparent Conducting Oxides for Application in Dye-Sensitized Solar Cells]*. Doctoral dissertation. Université de Nantes; 2011.
[6] Chang CC, Scarr N, Kumta PN. Synthesis and electrochemical characterization of $LiMO_2$ (M = Ni, $Ni_{0.75}Co_{0.25}$) for rechargeable lithium ion batteries. *Solid State Ionics*. 1998; 112(3-4): 329-344.
[7] Patil PS, Kadam LD. Preparation and characterization of spray pyrolyzed nickel oxide (NiO) thin films. *Applied Surface Science*. 2002; 199(1-4): 211-221.
[8] Wei X, Zhang QY, Zhou N, Peng B, Shen Y. Epitaxial growth of nano-texturized NiO films on MgO (001) substrates by a reactive magnetron sputtering method. *Journal of Crystal Growth*. 2024; 625: 127455.
[9] Dastan D, Shan K, Jafari A, Marszalek T, Mohammed MKA, Tao L, et al. Influence of heat treatment on H_2S gas sensing features of NiO thin films deposited via thermal evaporation technique. *Materials Science in Semiconductor Processing*. 2023; 154: 107232.
[10] Yu JH, Nam SH, Gil YE, Boo JH. The effect of ammonia concentration on the microstructure and electrochemical properties of NiO nanoflakes array prepared by chemical bath deposition. *Applied Surface Sciece*. 2020; 532: 147441.
[11] Bin Iqbal MS, Berry J, Ghosh K. Study of pure Ni, NiO, and mixture of Ni-NiO thin films on piezoelectric lithium niobate substrate by pulsed laser deposition. *Thin Solid Films*. 2023; 781: 140002.
[12] Hameed SA, Kareem MM, Khodair ZT, Saeed IMM. The influence of deposition temperatures on the structural and optical properties for NiO nanostructured thin films prepared via spray pyrolysis technique. *Chemical Data Collections*. 2021; 33: 100677.
[13] Lin YJ, Su TH, Kuo PC, Chang HC. A source of free holes in NiO thin films with different nickel content that are prepared using the sol-gel method. *Materials Chemistry and Physics*. 2022; 276: 125345.
[14] Klochko NP, Klepikova KS, Zhadan DO, Petrushenko SI, Kopach VR, Khrypunov GS, et al. Structure, optical, electrical and thermoelectric properties of solutionprocessed Li-doped NiO films grown by SILAR. *Materials Science in Semiconductor Processing*. 2018; 83: 42-49.
[15] Abdullah AR, El-Ashry MY, Duraia ESM, Mahmoud WE. The doping effect on the linear and nonlinear optical behaviors of nickel oxide films for multiple optoelectronic applications. *Micro and Nanostructures*. 2024; 188: 207785.
[16] Sahaa B, Sarkara K, Beraa A, Deba K, Thapac R. Schottky diode behaviour with excellent photoresponse in NiO/FTO heterostructure. *Applied Surface Science*. 2017; 418: 328-334.
[17] Alzahrani AOM, Abdel-Wahab MS, Alayash M, Aida MS. Metals and ITO contact nature on ZnO and NiO thin films. *Brazilian Journal of Physics*. 2021; 51(4): 1159-1165.
[18] Kaya D, Aydinoğlu HS, Tüzemen ES, Ekicibil A. Investigation of optical, electronic, and magnetic properties of p-type NiO thin film on different substrates. *Thin Solid Films*. 2021; 732: 138800.
[19] Kam V, Gawalt SK, Schwartz ES, Bocarsly J. Electrochemically active surface zirconium complexes on indium tin oxide. *Langmuir*. 1999; 15: 6598-6600.
[20] Sauter D, Weimar U, Noetzel G, Mitrovics J, Göpel W. Development of modular ozone sensor system for application in practical use. *Sensors and Actuators B: Chemical*. 2000; 69(1-2): 1-9.
[21] Beyer W, Hüpkes J, Stiebig H. Transparent conducting oxide films for thin film silicon Photovoltaics. *Thin Solid Films*. 2007; 516(2-4): 147-154.
[22] Granqvist CG, Hultåker A. Transparent and conducting ITO films: New developments and applications. *Thin Solid Films*. 2002; 411(1): 1-5.
[23] Antony A, Nisha M, Manoj R, Jayaraj MK. Influence of target to substrate spacing on the properties of ITO thin films. *Applied Surface Science*. 2004; 225(1-4): 294-301.
[24] Pissadakis S, Mallis S, Reekie L, Wikinson JS, Eason RW, Vainos NA, et al. Permanent holographic recording in indium oxide thin films using 193 nm excimer laser radiation. *Applied Physics A*. 1999; 69(3): 333-336.
[25] Zhang S. *Study of Fluorine-Doped Tin Oxide (FTO) Thin Films for Photovoltaics Applications*. PhD. Thesis. Université Grenoble Alpes; 2017.
[26] Wu S, Yuan S, Shi L, Zhao Y, Fang J. Preparation, characterization and electrical properties of fluorine-doped tin dioxide nanocrystals. *Journal of Colloid and Interface Science.* 2010; 346(1): 12-16.
[27] Noh SI, Ahn HJ, Riu DH. Photovoltaic property dependence of dye-sensitized solar cells on sheet resistance of FTO substrate deposited via spray pyrolysis. *Ceramics International*. 2012; 38(5): 3735-3739.

[28] Hudaya C, Jeon BJ, Lee JK. High thermal performance of SnO_2 : F thin transparent heaters with scattered metal nanodots. *ACS Appl Mater Interfaces*. 2015; 7(1): 57-61.
[29] Batzill M, Diebold U. The surface and materials science of tin oxide. *Progress in Surface Science*. 2005; 79(2-4): 47-154.
[30] Dauzhenka TA, Ksenevich VK, Bashmakov IA, Galibert J. Origin of negative magnetoresistance in polycrystalline SnO_2 films. *Physical Review B*. 2011; 83: 165309.
[31] Kaleli M, Aldemir DA, Bayram AB, Yavru CA. Structural, morphological, optical and electrical analysis of fluorine doped tin oxide thin films fabricated by ultrasonic spray pyrolysis. *Duzce University Journal of Science and Technology*. 2019; 7: 2107-2115.
[32] Colombel F, Castel X, Himdi M, Legeay G, Vigneron S, Cruz EM. Ultrathin metal layer, ITO film and ITO/Cu/ITO multilayer towards transparent antenna. *IET Science, Measurement & Technology*. 2009; 3(3): 229-234.
[33] Moholkar AV, Pawar SM, Rajpure KY, Bhosale CH. Effect of solvent ratio on the properties of highly oriented sprayed fluorine-doped tin oxide thin films. *Materials Letters*. 2007; 61(14-15): 3030-3036.
[34] Kim DH, Park MR, Lee HJ, Lee GH. Thickness dependence of electrical properties of ITO film deposited on a plastic substrate by RF magnetron sputtering. *Applied Surface Science*. 2006; 253(2): 409-411.
[35] Elangovan E, Ramamurthi K. Studies on micro-structural and electrical properties of spray-deposited fluorine-doped tin oxide thin films from low-cost precursor. *Thin Solid Films*. 2005; 476(2): 231-236.
[36] Li F, Chong C, Furui T, Chunxi L, Yue G, Shen L, et al. Semitransparent inverted polymer solar cells employing a sol-gel-derived TiO_2 electron-selective layer on FTO and MoO_3/Ag/MoO_3 transparent electrode. *Nanoscale Research Letters*. 2014; 9(1): 1-5.
[37] Abuelwafa AA, El-sadek A, Elnobi MS, Soga T. Effect of transparent conducting substrates on the structure and optical properties of tin (II) oxide (SnO) thin films: Comparative study. *Ceramics International*. 2021; 47(10): 13510-13518.
[38] Aouaj MA, Diaz R, Belayachi A, Rueda F, Abd-Lefdil M. Comparative study of ITO and FTO thin films grown by spray pyrolysis. *Materials Research Bulletin*. 2009; 44(7): 1458-1461.
[39] Hu Z, Zhang J, Hao Z, Hao Q, Geng X, Zhao Y. Highly efficient organic photovoltaic devices using F-doped SnO_2 anodes. *Applied Physics Letters*. 2011; 98(12): 66.
[40] Suryanarayana B, Ramanjaneyulu K, Raghavendra V, Murali N, Parajuli D, Mulushoa SY, et al. Effect of Sm^{3+} substitution on dc electrical resistivity and magnetic properties of Ni-Co ferrites. *Journal of the Indian Chemical Society*. 2022; 99(8): 100623.
[41] Kumar SR, Priya GV, Aruna B, Raju MK, Parajuli D, Murali N, et al. Influence of Nd^{3+} substituted $Co_{0.5}Ni_{0.5}Fe_2O_4$ ferrite on structural, morphological, dc electrical resistivity and magnetic properties. *Inorganic Chemistry Communications*. 2022; 136: 109132.
[42] Geetha P, Taddesse P, Murali N, Narayana PL. Impact of Gd^{3+} and Nd^{3+} ions substitution on structural and magnetic properties of $Co_{0.5}Ni_{0.5}Fe_2O_4$ ferrite system. *Journal of the Indian Chemical Society*. 2022; 99(1): 100255.
[43] Tauc J, Menth A. States in the gap. *Journal of Non-Crystalline Solids*. 1972; 8-10: 569.
[44] Urbach F. The long-wavelength edge of photographic sensitivity and of the electronic absorption of solids. *Physical Review Journals Archive*. 1953; 92(5): 1324.
[45] Vettumperumal R, Kalyanaraman S, Santoshkumar B, Thangavel R. Estimation of electron-phonon coupling and Urbach energy in group-I elements doped ZnO nanoparticles and thin films by sol-gel method. Mater. *Materials Research Bulletin*. 2016; 77: 101-110.
[46] Singha J, Verma V, Kumar R, Kumara R. Influence of Mg^{2+}-substitution on the optik bant boşluk enerjisi $Cr_{2-x}Mg_xO_3$ nanoparticles. *Results in Physics*. 2009; 13: 102106.
[47] Mesrouk M. *Etude d'une électrode tri-couches à base de TCO/Métal/TCO pour une céllule solaire organique [Study of a Triple-Layer Electrode Based on TCO/Metal/TCO for an Organic Solar Cell]*. Doctoral dissertation. Université Mouloud Mammeri; 2013.
[48] Rödl C, Schleife A. Photoemission spectra and effective masses of n-and p-type oxide semiconductors from first principles: ZnO, CdO, SnO_2, MnO, NiO. *Physica Status Solidi (A)*. 2014; 211(1): 74-81.
[49] Sze SM, Li Y, Kwok KN. *Physics of Semiconductor Devices*. New York: John Wiley & Sons; 2021. p.994.
[50] Stamataki M, Sargentis C, Tsamakis D, Fasaki I, Kompitsas M. Hydrogen gas sensing application of Al/NiO schottky diode. In: *Sensors*. Lecce, Italy: IEEE; 2008. p.843-846.
[51] Castro-Hurtado I, Malagù C, Morandi S, Pérez N, Mandayo GG, Castaño E. Properties of NiO sputtered thin films and modeling of their sensing mechanism under formaldehyde atmospheres. *Acta Materialia*. 2013; 61(4): 1146-1153.

[52] Saju J, Balasundaram ON. Optimization and characterization of NiO thin films prepared via NSP technique and its P-N junction diode application. *Materials Science-Poland*. 2019; 37(3): 338-346.
[53] Kara İ, Alhasani DMH, Kayiş AF, Yalçinkaya Ö, Gençyilmaz O, Hafedh AIR. ZnO/ITO, Sn and Cu doped ZnO/ITO films as an photoanode for solar cell: Production and characterizations. *Yuzuncu Yil University Journal of TheInstitute of Natural and Applied Sciences*. 2024; 29(1): 447-457.
[54] Bhujel K, Thangavel R, Pal KK, Sardar P, Nayak D, Singh NS, et al. Cu-doped NiO thin film's structural, optical, and electrical properties and its negative absorption behaviour in the Infra-Red region. *Physica B: Condensed Matter*. 2024; 668: 416129.
[55] Mistry BV, Bhatt P, Bhavsar KH, Trivedi SJ, Trivedi UN, Joshi US. Growth and properties of transparent p-NiO/n-ITO(In_2O_3 : Sn) p-n junction thin film diode. *Thin Solid Films*. 2011; 519(11): 3840-3843.